Published in "Journal of Physics: Condensed Matter 31(48): 485705, 2019"
which should be cited to refer to this work.

Persistent antiferromagnetic order in heavily overdoped $Ca_{1-x}La_xFeAs_2$

Edoardo Martino[1,4,6], Maja D Bachmann[4], Lidia Rossi[1], Kimberly A Modic[4], Ivica Zivkovic[2], Henrik M Rønnow[2], Philip J W Moll[3,4], Ana Akrap[5], László Forró[1] and Sergiy Katrych[1]

[1] Laboratory of Physics of Complex Matter, Institute of Physics, École Polytechnique Fédérale de Lausanne (EPFL), CH-1015 Lausanne, Switzerland
[2] Laboratory for Quantum Magnetism, Institute of Physics, Ecole Polytechnique Féderale de Lausanne (EPFL), CH-1015 Lausanne, Switzerland
[3] Laboratory for Quantum Materials, Institute of Materials, École Polytechnique Fédérale de Lausanne (EPFL), CH-1015 Lausanne, Switzerland
[4] Max Planck Institute for Chemical Physics of Solids, D-01187 Dresden, Germany
[5] Department of Physics, University of Fribourg, CH-1700 Fribourg, Switzerland

E-mail: edoardo.martino@epfl.ch

Abstract

In the $Ca_{1-x}La_xFeAs_2$ (1 1 2) family of pnictide superconductors, we have investigated a highly overdoped composition ($x = 0.56$), prepared by a high-pressure, high-temperature synthesis. Magnetic measurements show an antiferromagnetic transition at $T_N = 120$ K, well above the one at lower doping ($0.15 < x < 0.27$).

Below the onset of long-range magnetic order at T_N, the electrical resistivity is strongly reduced and is dominated by electron–electron interactions, as evident from its temperature dependence. The Seebeck coefficient shows a clear metallic behavior as in narrow band conductors. The temperature dependence of the Hall coefficient and the violation of Kohler's rule agree with the multiband character of the material. No superconductivity was observed down to 1.8 K. The success of the high-pressure synthesis encourages further investigations of the so far only partially explored phase diagram in this family of Iron-based high temperature superconductors.

Keywords: magnetism, iron-based superconductor, transport properties, high-pressure synthesis, antiferromagnet

(Some figures may appear in colour only in the online journal)

Introduction

Since the discovery of high temperature superconductivity in the pnictides [1], numerous compounds have been synthesized, notably the families: $(Ba,K)Fe_2As_2$ (1 2 2) [2], FeSe (11) [3], LiFeAs (1 1 1) [4], $LaFeAsO_{1-x}(H,F)_x$ (1 1 1 1) [1], and most recently, the $Ca_{1-x}La_xFeAs_2$ (1 1 2) [5]. The 1 1 2-family distinguishes itself from the others by having a metallic block-layer between the FeAs planes. Such metallic layer, made of As zig-zag chains (figure 1(A)) [5], adds one hole-like pocket and four bands with a Dirac-cone-like dispersion to the band structure [6]. It is claimed that the possible coexistence of Dirac electrons and superconductivity in the FeAs layers, can potentially lead to the observation of Majorana fermions [7]. The other striking peculiarity of the $Ca_{1-x}La_xFeAs_2$ 1 1 2-family becomes apparent in its temperature-doping phase diagram. It is only partially explored, as only the doping range $0.15 < x < 0.27$ has been synthesised to date, marked as the solid background area in figure 1(B). It is known that in $Ca_{1-x}La_xFeAs_2$ superconductivity appears with its highest observed critical temperature of $T_C = 35$ K for the lowest reported doping level ($x = 0.15$). For higher doping, T_C decreases until its full suppression at $x = 0.23$. Collinear antiferromagnetic order (AFM) coexists

[6] Author to whom all correspondence should be addressed.

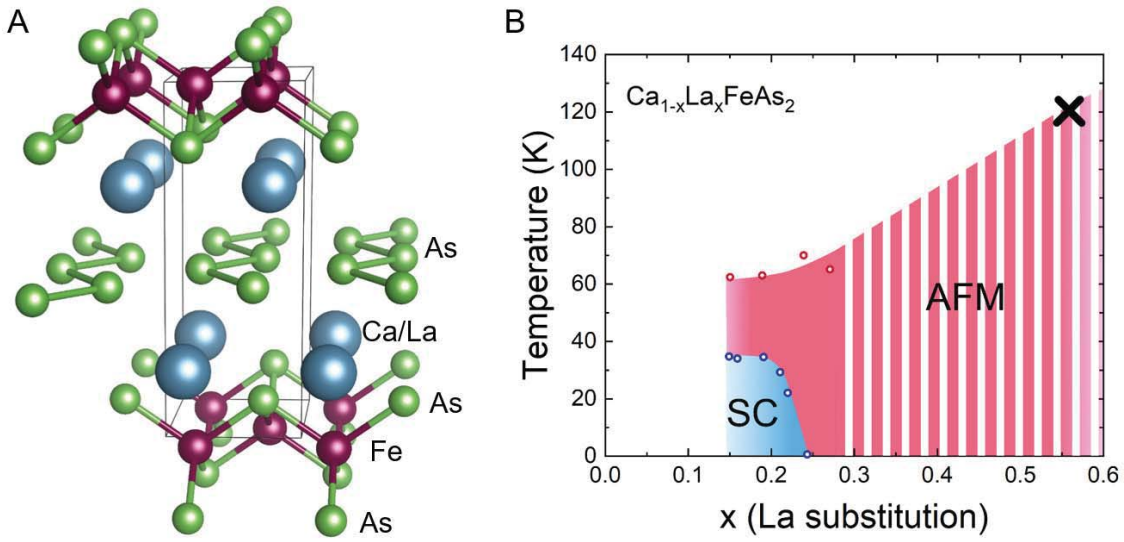

Figure 1. (A) Sketch of the $Ca_xLa_{1-x}FeAs_2$ crystal structure. (B) The proposed electronic phase diagram for $Ca_xLa_{1-x}FeAs_2$ as a function of the substitutional doping. Data from previously reported synthesis are shown as open circles in the region with solid background, for $0.15 < x < 0.27$ [9]. The black cross is the result of the present study, showing the antiferromagnetic transition temperature (120 K) for $x = 0.56$. Striped area is an extrapolation of the AFM phase.

microscopically with superconductivity [8, 9] in the doping range of $0.15 < x < 0.23$. The Néel temperature (T_N) constantly increases with doping, even beyond the suppression of the superconducting phase [9].

The magnetic order goes hand-in-hand with a structural phase transition, from monoclinic to triclinic symmetry, which is driven by magneto-elastic coupling [8], a common feature in the pnictides [10]. Another commonality among the pnictide families is the manifestation of a kink in the temperature dependence of the electrical resistivity at the transition [10]. This is due to reduced scattering from magnetic fluctuations below T_N [8].

For a better understanding of this family, and the pnictide superconductors in general, it is important to explore the phase diagram in a broad doping range, especially on the overdoped side, above $x = 0.27$. It would be highly informative to check if there is a second superconducting dome, as in the 1 1 1 1-family [11], and to see how the AFM evolves with increasing carrier density.

In this quest, we used high-pressure synthesis to make heavily over-doped single crystals of $Ca_{1-x}La_xFeAs_2$. Structural refinement of single crystal x-ray diffraction (XRD) data yields $x = 0.56$. Magnetization, XRD and resistivity measurements suggest that the antiferromagnetic phase transition occurs around 120 K. Transport measurements show bad metal behaviour, with strong interband scattering, and no superconducting transition was observed down to 1.8 K.

Our measurements add an important point to the phase diagram of the 1 1 2-family (figure 1(B)), suggesting the persistence of the AFM order even at higher doping levels. Compared to other pnictides families, in 1 1 2-family the AFM order persists over a considerably wider doping range [12, 13].

High-pressure synthesis

High-pressure, high-temperature synthesis proved to be a valuable approach to obtain novel materials and to stabilize phases and compositions that are not accessible by other crystal growth techniques [14–16]. Another advantage of the high-pressure synthesis is that the chemical reaction happens in a strongly confined space. If the reaction were prepared inside a quartz ampulla for example, because As has a high vapour pressure, the developing overpressure at high temperatures could lead to an explosion.

For the high-pressure synthesis, 0.6 g mixture of starting components were used. As, Ca, CaO, FeAs, La, respectively with the molar ratio of 1:0.6:1:2:0.4 were placed in a BN crucible with 0.4 g of NaCl flux. The reactants were pressurized at 3 GPa and then heated to 1430 °C within 2 h. The temperature was maintained for 5 h, then slowly (7.5 °C h^{-1}) cooled down to 1000 °C and annealed at this temperature for 2 h. Afterwards, the system was rapidly cooled down to room temperature by switching off the power supply. The NaCl flux was dissolved in distilled water. Plate-like single crystals, of $Ca_{1-x}La_xFeAs_2$, with approximate dimensions of $10 \times 120 \times 180$ μm^3 were selected for further investigations. In addition, a large number of small crystallites of FeAs phase were formed as well.

Single crystal XRD

The two majority phases of FeAs and $Ca_{1-x}La_xFeAs_2$ were identified by Rietveld analysis of the powder XRD spectra, with mass ratios of 14% and 86%, respectively (figure 2(A)). Single crystal XRD was performed on selected crystals of $Ca_{1-x}La_xFeAs_2$. The diffraction pattern was collected using a SuperNova (dual Source) four-circle diffractometer (Agilent Technologies, USA) equipped with a CCD detector. Data reduction and analytical absorption correction were made using the CrysAlis^{Pro} software package (Oxford diffraction, 2014). The crystal structure was refined using known lattice parameters from [5] and the SCHELXL software package. The refinement of the spectra indicates a composition of

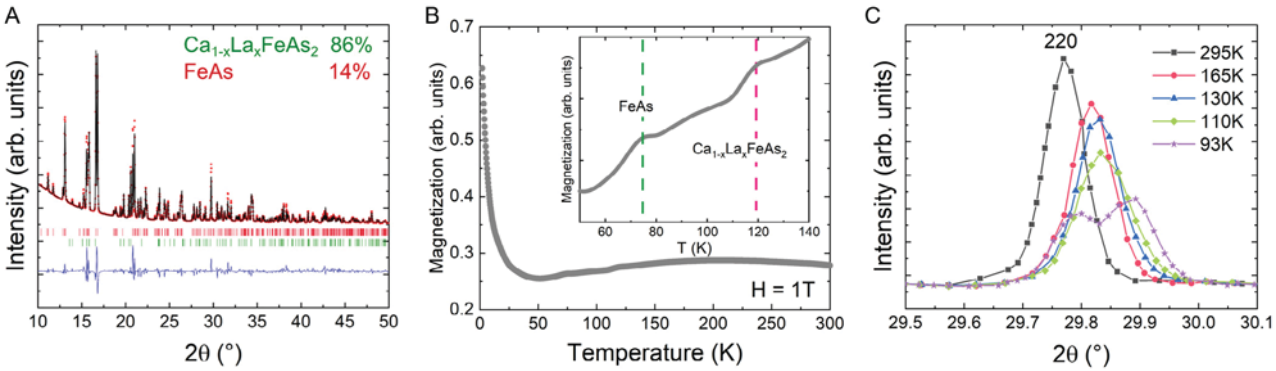

Figure 2. (A) Powder XRD and Rietveld refinement for the reaction products. (B) Magnetization temperature dependence of the mixture of FeAs and overdoped $Ca_{1-x}La_xFeAs_2$. The inset shows an enlarged view of magnetic transitions of FeAs at 77 K (green) and $Ca_{1-x}La_xFeAs_2$ at ~120 K (pink). (C) The temperature dependence of the 2 2 0 diffraction peak (measured with $\lambda = 0.71446$ Å) shows a splitting which occurs between 110 K and 93 K as a consequence of the monoclinic to triclinic phase transition, provoked by the magneto-elastic coupling in the AFM state.

Table 1. Results of the structural refinement of $Ca_{0.44}La_{0.56}FeAs_2$.

Crystal size	$10 \times 119 \times 180$ μm^3	
Empirical formula	$Ca_{0.44}La_{0.56}FeAs_2$	
Temperature	293(2) K	
Crystal symmetry	Monoclinic	
Space group	$P2_1$	
Unit cell dimensions	$a = 3.9463(7)$ Å	$\alpha = 90°$
	$b = 3.9247(5)$ Å	$\beta = 90.792(15)°$
	$c = 10.4652(18)$ Å	$\gamma = 90°$
Volume	162.07(5) $Å^3$	
Density (calculated)	6.180 Mg m^{-3}	
Refinement method	Full-matrix least-squares on F^2	
Goodness-of-fit on F^2	1.081	
Final R indices [$I > 2$ sigma(I)]	$R_1 = 0.0743$, w$R_2 = 0.1956$	
R indices (all data)	$R_1 = 0.0809$, w$R_2 = 0.2018$	

$x = 0.56(1)$. On the very same crystal, energy-dispersive x-ray spectroscopy (EDX), gave $x = 0.57(2)$. For the many different crystals synthesised, EDX gave a slight variation in the composition in the $0.53 < x < 0.6$ range. The main quantities deduced from single crystal XRD are shown in table 1.

The antiferromagnetic state

The magnetic state of overdoped $Ca_{1-x}La_xFeAs_2$ was determined by the temperature-dependent magnetization (figure 2(B)) which was measured in a MPMS SQUID. The data were collected in field cooling of 1 T. To enhance the signal, 14 mg of selected reaction products were introduced in a gelatine capsule for measurement, which contained randomly oriented crystals of $Ca_xLa_{1-x}FeAs_2$ and FeAs as impurity phase. Two kinks are present in the magnetization measurement, one around 77 K and the other around 120 K. The kink at 77 K is associated with the magnetic transition present in FeAs [17]. The broad kink at higher temperature is compatible with the antiferromagnetic transition in $Ca_xLa_{1-x}FeAs_2$. Previously reported magnetization data on single crystals show a different shape of the kink for different field orientations [8]. Since the sample we use for magnetic measurements is a collection of differently oriented crystallites, such anisotropic response is averaged, resulting in a smeared and less sharp kink. The small variation in composition in the range from $x = 0.55$ to $x = 0.6$ also contributes to the observed magnetization curve.

Another signature of the AFM state, observed in a previous investigation of $Ca_xLa_{1-x}FeAs_2$, is the lowering of the crystal symmetry from monoclinic to triclinic [18], via a magneto-elastic coupling. In order to verify this, around 20 single crystals of $Ca_{1-x}La_xFeAs_2$ were assembled in a glass capillary for temperature-dependent XRD measurements, performed with synchrotron radiation at the BM01 station of the Swiss-Norwegian Beam Lines (ESRF, Grenoble, France). The data were collected with Pilatus@SNBL diffractometer, and processed with SNBL ToolBox software [20]. The results in figure 2(B), show the evolution of the 2 2 0 Bragg peak with temperature. At room temperature, a single resolution-limited peak is observed at $2\Theta = 29.77°$. At lower temperatures, the peak shifts to higher 2Θ values due to the contraction of the unit cell. When the temperature is brought below T_N, the peak splits into two overlapping peaks, indicating that the symmetry is lowered (figure 2(C)) from monoclinic to triclinic. The difference in transition temperature compared to magnetization measurements may be due to the different doping level of the selected crystals.

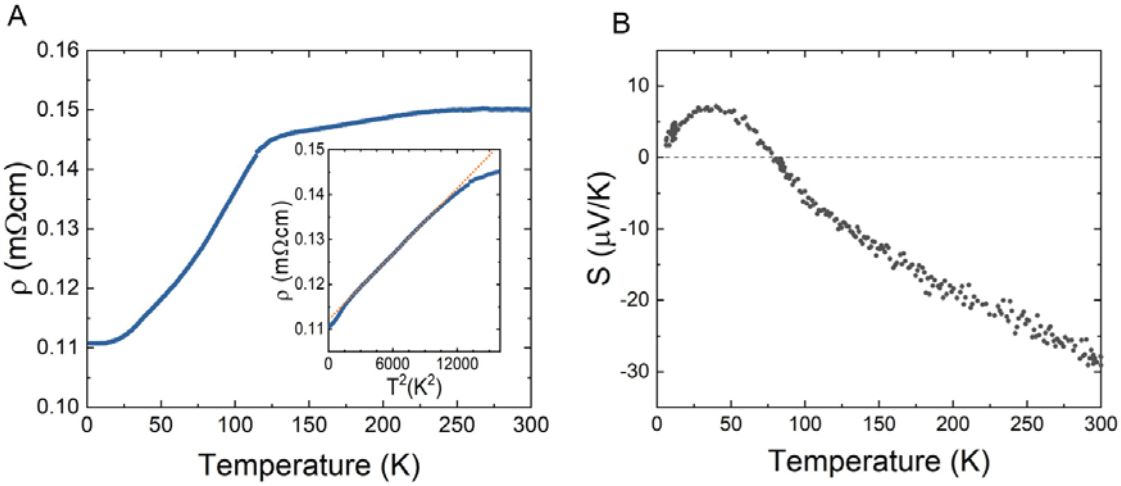

Figure 3. (A) Temperature dependence of the in-plane electrical resistivity, measured on a FIB micro-fabricated single crystal. Inset: The low temperature resistivity ($T < 90$ K) plotted as a function of T^2. The dotted orange line is a guide for the eyes. (B) Seebeck coefficient versus temperature measured on a pellet sample of the overdoped $Ca_xLa_{1-x}FeAs_2$ ($0.55 < x < 0.6$).

Further indication of long range magnetic order bellow T_N is given by the temperature dependence of electrical resistivity, discussed in the next section, as a sharp change in the slope is evident around 120 K (figure 3(A)). Resistivity is sensitive to the suppression of the scattering on magnetic fluctuations that occur at the paramagnetic-to-antiferromagnetic transition temperature, because the long range magnetic order weakly scatters conduction electrons. The combined experimental evidence supports the proposed manifestation of AFM around 120 K, in heavily overdoped $Ca_{1-x}La_xFeAs_2$.

Transport properties

Electrical resistivity was measured on single crystals of well-defined composition. The phase purity and doping level were characterized by single crystal XRD and EDX. Using a focused ion beam (FIB), the single crystal was micro-fabricated into a Hall-bar geometry of size $110 \times 11 \times 6$ μm^3 [21]. In this way the current path was defined along the *ab*-plane for in-plane resistivity (ρ), magnetoresistance and Hall coefficient (R_{Hall}) measurements. The temperature dependence of the in-plane electrical resistivity is shown in figure 3(A). The precise geometry of the micro-fabricated sample enabled to measure the resistivity with high accuracy. Our sample shows a lower resistivity compared to the reported results for a lower doping level ($x = 0.27$) [8]. This could be attributed to the increased carrier density accompanying the overdoping, as observed in other pnictides [22]. On cooling, ρ(T) shows a weak temperature dependence down to 120 K, followed by a kink at the paramagnetic-AFM transition temperature. Below 120 K, the behaviour is more metallic but the residual resistivity (ρ_0) is relatively high. At this point, the origin of ρ_0 is unclear. One possibility is that it comes from static disorder introduced during the high-pressure synthesis.

The temperature dependence of ρ in a broad range (between 35 K and 90 K) shows a T^2 behaviour, which could be interpreted as Fermi-liquid-like and described by $\rho(T) = \rho_0 + AT^2$ (with $\rho_0 = 0.11$ mΩ cm and $A = 0.0024$ μΩ cm K^{-2}) (inset to figure 3(A)). It is challenging to understand ρ(T) above the magnetic transition ($T > T_N$), where it shows a very weak temperature dependence. This bad metal character is in contrast with the Seebeck coefficient (figure 3(B)) which displays a clear metallic dependence in the same temperature range. We propose that this behaviour originates from the increasing interband scattering with decreasing temperatures, reducing the resistivity temperature dependence, which opposes the effect of electron-phonon scattering. A similar mechanism was reported for other pnictides where multiple bands at the chemical potential favour strong interband scattering [23].

It has to be mentioned that the Mooij correlation is another possible source of the observed flat resistivity above $T > T_N$ [24]. In the case of a high concentration of static defects, marked by the elevated ρ_0, electronic interferences between the scattering events tend to weakly localize electrons. After a threshold value ρ_{TH}, even the $d\rho/dT$ changes to a negative value. In Mooij's original picture, ρ_{TH} was equal to 0.2 mΩ cm (close to the value in figure 3(A), 0.15 mΩ cm), but later on Tsuei [25] showed that ρ_{TH} is a material dependent quantity. In our case, ρ_0 is indeed high, however, if localization effects dominate, one would not expect a major change in ρ(T) at T_N. Due to the strong change in the slope below T_N, we believe that the multiband scattering dominates the high temperature resistivity.

The temperature dependence of the Seebeck coefficient (S) (figure 3(B)) may provide a further insight into the electronic properties of the material. In multiband systems, the Seebeck coefficient is given by $S = \frac{\sum_i \sigma_i S_i}{\sum_i \sigma_i}$, where σ_i is the ith-band conductivity and S_i is its thermoelectric contribution, positive for holes and negative for electrons. The Seebeck coefficient is an open-circuit measurement, so it is not affected by grain boundaries or static defects, but, in order to obtain a precise measurement, one needs a well-defined linear temperature gradient on the sample, hence a sample much longer than the typical 100 μm size. For this reason, many small size single crystals were compressed into a pellet, from which a millimeter long bar was shaped, and used for the measurement.

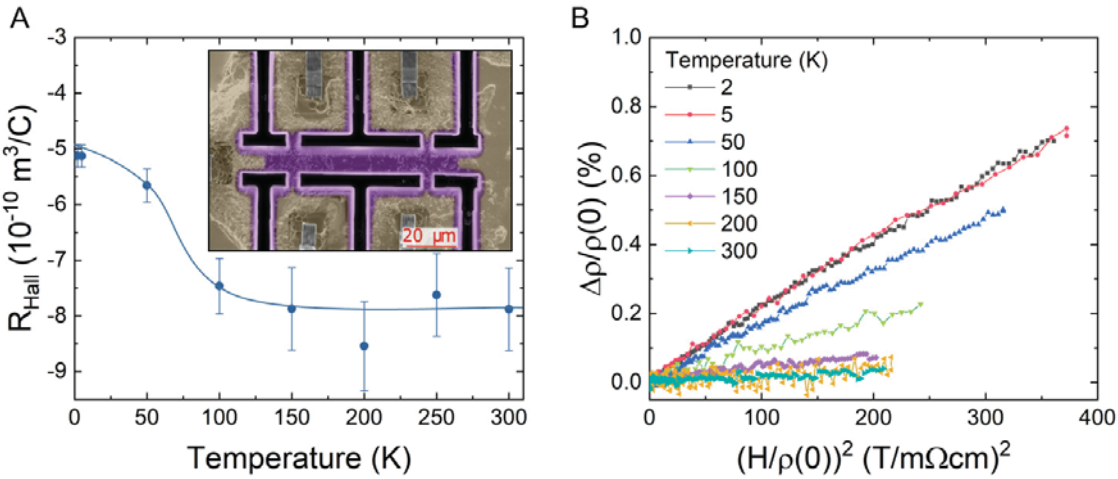

Figure 4. (A) Temperature dependence of the Hall coefficient, (the blue line is added as guide for the eyes). In the inset, the SEM picture shows the micro-structured sample. False colors are added to highlight the sample (purple). The sputtered gold layer (yellow) and the FIB-deposited Pt leads (gray) give the electrical contacts. (B) Kohler plot of the magnetoresistance plotted at fix temperatures.

The negative Seebeck coefficient at high temperatures suggests a dominant contribution of electrons, in agreement with the Hall coefficient (see figure 4(A)) and previous reports for samples with low doping [18]. The high temperature part is linear, and by using the Mott's formula: $S(T) = \frac{\pi^2}{3}\left(\frac{k_B}{e}\right)\left(\frac{T}{T_F}\right)$, we extract an effective Fermi temperature (T_F) of 3080 K (0.27 eV). The T_F value and the A coefficient extracted from the resistivity temperature dependence fall on the same trend as a number of Fermi liquids, probing the relationship between the electron–electron scattering rate and Fermi energy [19]. This magnitude of T_F suggests a relatively narrow conduction band. Just below the transition temperature, S changes sign, as R_H increases, revealing an increased contribution of the hole bands to the overall conductivity. The additional hole pocket induced by the As-chains could be responsible for these observations.

Below T_N, $S(T)$ changes slope, as it is defined by the energy dependence of the scattering rate, which is affected by the magnetic order and the Fermi surface reconstruction. Below this temperature, the relative contributions of the electron and hole bands change, and S changes sign. This is yet another manifestation of the multiband character of the material. In the $T \to 0$ K limit, S goes to 0, as required by thermodynamics [26].

Magneto-transport properties

The Hall coefficient (R_H) (figure 4(A)) was measured on the same sample as the electrical resistivity. Its sign corroborates with that of S at room temperature, confirming that the electron-band dominate the transport properties. R_H shows a weak temperature dependence, similar to that of the less doped samples [18]. Its absolute value at 300 K ($-8\ 10^{-10}$ m^3 C^{-1}) is much lower than that of the $x = 0.23$ doping level ($-23\ 10^{-9}$ m^3 C^{-1}) [18], and it is consistent with the higher electron doping level. The extracted charge carrier density is $7.8\ 10^{21}$ cm^{-3}, but it should be taken with caution due to the multiband character of the material. With the same reserve, one can calculate the carrier mobility which comes up to $\mu_H = R_H/\rho = 5.3\,\text{cm}^2\ \text{V}^{-1}\ \text{s}^{-1}$, a relatively low value for a metal.

The longitudinal magnetoresistance ($B \| c$-axis, j in the ab-plane) is quadratic in field in the whole temperature range (figure 4(B)) as expected for a metal, especially in the low field limit ($\mu_H B \ll 1$). The data plotted in Kohler's representation shows that they do not fall on a single line, which would be expected for simple metals with a single isotropic relaxation time. It is quite natural that $Ca_{1-x}La_xFeAs_2$ disobeys the Kohler's law since it has multiple bands taking part in the electronic conduction, with possibly multiple and anisotropic scattering times. The same behaviour is also evident for lower doping levels and in other pnictides [27, 28].

Conclusions

By growing $Ca_{1-x}La_xFeAs_2$ ($x = 0.56$), we have demonstrated that high-pressure synthesis could be the route for exploring the heavily overdoped side of the 1 1 2-family phase diagram. Using synchrotron XRD, magnetic susceptibility and transport measurements, the sample was characterized in detail. We have identified a paramagnet-to-antiferromagnet transition around 120 K, well above the highest previously reported transition temperature of 70 K for doping level of $x = 0.27$. This result suggests a monotonous increase of the antiferromagnetic ordering strength with doping, which is a unique feature among the iron-based superconductors. Such peculiar behaviour as function of doping might be related to the existence of metallic block-layers of As zig-zag chains in the 1 1 2-family [9]. The enlarged Fermi surface with doping could enhance the Fermi surface nesting which in turn, increases the antiferromagnetic coupling [29, 30].

Acknowledgments

We thank Konstantin Semeniuk and Mathieu François Padlewski for useful discussions.

The work at the Laboratory of Physics of Complex Matter was supported by the Swiss National Science Foundation through its SINERGIA network MPBH and Grant No. 200021_175836. Ana Akrap acknowledges funding from the Swiss National Science Foundation through project PP00P2 170544.

Synchrotron XRD measurement was performed at the BM01 station of the Swiss-Norwegian Beam Lines of the European Synchrotron Radiation Facility (ESRF, Grenoble, France).

ORCID iDs

Edoardo Martino https://orcid.org/0000-0001-9654-9820
Maja D Bachmann https://orcid.org/0000-0002-1075-3888
Ana Akrap https://orcid.org/0000-0003-4493-5273

References

[1] Kamihara Y, Watanabe T, Hirano M and Hosono H 2008 Iron-based layered superconductor La $[O_{1-x}F_x]$ FeAs ($x = 0.05$–0.12) with $T_c = 26$ K *J. Am. Chem. Soc.* **130** 3296

[2] Rotter M, Tegel M and Johrendt D 2008 Superconductivity at 38 K in the iron arsenide $(Ba_{1-x}K_x)Fe_2As_2$ *Phys. Rev. Lett.* **101** 107006

[3] Hsu F C *et al* 2008 Superconductivity in the PbO-type structure α-FeSe *Proc. Natl Acad. Sci.* **105** 14262

[4] Tapp J H, Tang Z, Lv B, Sasmal K, Lorenz B, Chu P C and Guloy A M 2008 LiFeAs: an intrinsic FeAs-based superconductor with $T_c = 18$ K *Phys. Rev.* B **78** 060505

[5] Katayama N *et al* 2013 Superconductivity in $Ca_{1-x}La_xFeAs_2$: a novel 1 1 2-type iron pnictide with arsenic zigzag bonds *J. Phys. Soc. Japan* **82** 123702

[6] Wu X, Le C, Liang Y, Qin S, Fan H and Hu J 2014 Effect of As-chain layers in $CaFeAs_2$ *Phys. Rev.* B **89** 205102

[7] Wu X, Qin S, Liang Y, Le C, Fan H and Hu J 2015 $CaFeAs_2$: a staggered intercalation of quantum spin Hall and high-temperature superconductivity *Phys. Rev.* B **91** 081111

[8] Jiang S *et al* 2016 Structural and magnetic phase transitions in $Ca_{0.73}La_{0.27}FeAs_2$ with electron-overdoped FeAs layers *Phys. Rev.* B **93** 054522

[9] Kawasaki S, Mabuchi T, Maeda S, Adachi T, Mizukami T, Kudo K, Nohara M and Zheng G Q 2015 Doping-enhanced antiferromagnetism in $Ca_{1-x}La_xFeAs_2$ *Phys. Rev.* B **92** 180508

[10] Ishida K, Nakai Y and Hosono H 2009 To what extent iron-pnictide new superconductors have been clarified: a progress report *J. Phys. Soc. Japan* **78** 062001

[11] Iimura S, Matsuishi S, Sato H, Hanna T, Muraba Y, Kim S W, Kim J E, Takata M and Hosono H 2012 Two-dome structure in electron-doped iron arsenide superconductors *Nat. Commun.* **3** 943

[12] Hosono H and Kuroki K 2015 Iron-based superconductors: current status of materials and pairing mechanism *Physica* C **514** 399

[13] Canfield P C and Bud'Ko S L 2010 FeAs-based superconductivity: a case study of the effects of transition metal doping on $BaFe_2As_2$ *Annu. Rev. Condens. Matter Phys.* **1** 27–50

[14] Karpinski J, Zhigadlo N D, Katrych S, Puzniak R, Rogacki K and Gonnelli R 2007 Single crystals of MgB2: Synthesis, substitutions and properties *Physica* C **456** 3

[15] Zhigadlo N D, Katrych S, Bukowski Z, Weyeneth S, Puzniak R and Karpinski J 2008 Single crystals of superconducting $SmFeAsO_{1-x}F_y$ grown at high pressure *J. Phys.: Condens. Matter* **20** 342202

[16] Martino E *et al* 2018 $Sr_2Pt_{8-x}As$: a layered incommensurately modulated metal with saturated resistivity *IUCrJ* **5** 470

[17] Segawa K and Ando Y 2009 Magnetic and transport properties of FeAs single crystals *J. Phys. Soc. Japan* **78** 104720

[18] Caglieris F *et al* 2016 Research update: structural and transport properties of (Ca, La) $FeAs_2$ single crystal *APL Mater.* **4** 020702

[19] Lin X, Fauqué B and Behnia K 2015 Scalable T_2 resistivity in a small single-component Fermi surface *Science* **349** 945–8

[20] Dyadkin V, Pattison P, Dmitriev V and Chernyshov D 2016 A new multipurpose diffractometer PILATUS@ SNBL *J. Synchrotron Radiat.* **23** 825

[21] Moll P J 2018 Focused ion beam microstructuring of quantum matter *Ann. Rev. Condens. Matter Phys.* **9** 147–62

[22] Rullier-Albenque F, Colson D, Forget A and Alloul H 2009 Hall effect and resistivity study of the magnetic transition, carrier content, and Fermi-liquid behavior in Ba $(Fe_{1-x}Co_x)_2As_2$ *Phys. Rev. Lett.* **103** 057001

[23] Akrap A, Dai Y M, Wu W, Julian S R and Homes C C 2014 Optical properties and electronic structure of the nonmetallic metal FeCrAs *Phys. Rev.* B **89** 125115

[24] Mooij J H 1973 Electrical conduction in concentrated disordered transition metal alloys *Phys. Status Solidi* a **17** 521–30

[25] Tsuei C C 1986 Nonuniversality of the Mooij correlation—the temperature coefficient of electrical resistivity of disordered metals *Phys. Rev. Lett.* **57** 1943

[26] Chaikin P M 1990 An introduction to thermopower for those who might want to use it to study organic conductors and superconductors *Organic Superconductivity* (Boston, MA: Springer) pp 101–15

[27] Pisoni A, Szirmai P, Katrych S, Náfrádi B, Gaál R, Karpinski J and Forró L 2016 Magnetotransport studies of superconducting $Pr_4Fe_2As_2Te_{1-x}O_4$ *Phys. Rev.* B **93** 094519

[28] Xing X, Xu C, Li Z, Feng J, Zhou N, Zhang Y, Sun Y, Zhou W, Xu X and Shi Z 2017 Angular-dependent magnetoresistance study in $Ca_{0.73}La_{0.27}FeAs_2$: a 'parent' compound of 1 1 2-type iron pnictide superconductors *J. Phys.: Condens. Matter* **30** 025701

[29] Li M Y *et al* 2015 Significant contribution of As 4 p orbitals to the low-lying electronic structure of the 1 1 2-type iron-based superconductor $Ca_{0.9}La_{0.1}FeAs_2$ *Phys. Rev.* B **91** 045112

[30] Onari S, Yamakawa Y and Kontani H 2014 High-T_c superconductivity near the anion height instability in Fe-based superconductors: analysis of $LaFeAsO_{1-x}H_x$ *Phys. Rev. Lett.* **112** 187001